Application of track-before-detect techniques in GNSS-based passive radar for maritime surveillance

Fabrizio Santi and Debora Pastina
Department of Information Engineering, Electronics and Telecommunications, Sapienza University of Rome
Via Eudossiana, 18 – 00184 – Rome, Italy
fabrizio.santi@uniroma1.it; debora.pastina@uniroma1.it

***Abstract*—GNSS-based passive radar has been recently proved able to enable moving target detection in maritime surveillance applications. The main restriction lies in the low Equivalent Isotropic Radiated Power (EIRP) level of navigation satellites. Extending the integration times with proper target motion compensation has been shown to be a viable solution to improve ship detectability, but this involves computational complexity and increasing sensitivity to motion model mismatches. In this work, we consider the application of a Track-Before-Detect (TBD) method to considerably increase the integration time (and therefore the detection capability) at the same time keeping the computational complexity affordable by practical systems. Dynamic programming TBD algorithms have been specialized for the considered framework and tested against experimental dataset. The obtained results show the effectiveness of this approach to improve the detection capability of the system despite the restricted power budget.**

Keywords—GNSS-based passive radar, long-integration time, track-before-detect, maritime surveillance

I. INTRODUCTION

Since many years, Global Navigation Satellite System (GNSS) signals have been considered as opportunistic sources for passive radar systems. One of the most recent applications of this technology concerns the maritime surveillance, where it can be regarded as a very appealing and prospective solution [1,2]. In fact, as well as the known benefits deriving from the lack of dedicated transmitters, GNSS-based passive radar can rely on highly precise synchronized and ubiquitous electromagnetic sources, illuminating both coastal and open sea areas. It is worth to explicitly point out that areas far from land are in the scope of coverage of few satellite sources, where GNSS can benefit of relatively large bandwidths (e.g. around 10 MHz for Galileo E5a/b or GPS L5 signals) offering resolutions comparable or even smaller than the size of typical maritime targets. Moreover, navigation satellites constellations are designed such that each point over the Earth 'surface is constantly illuminated by a large number of satellites (typically around 24 by considering GPS, GLONASS, Galileo and BeiDou), so that multistatic operations can be applied to improve the detection and localization capabilities of the system [3,4].

The main drawback of this technology is represented by the low level of flux power density reaching the sea surface, making challenging the detection of far and/or small ships. To enable the detection of the low observable targets, in [2] long-integration time Moving Target Indication (MTI) techniques have been developed to integrate the received signal energy over multiple short time frames, thus reaching dwells in the order of tens of seconds, by proper compensation of the motion of the hypothesized targets. The theoretical and experimental results therein provided showed that such long dwells are a mandatory condition to enable the detection of the targets of interest.

While also multistatic approaches have been investigated to improve the signal-to-noise ratio (SNR) [4], further extending the integration time appears being the natural solution to improve the probability of detection. In principle, this could be obtained by straightforwardly increasing the number of considered frames, but at the cost of a considerable higher computational complexity: this conflicts with the need of a data processing light enough for its implementation in surveillance systems able to provide outputs in near real time mode. Not to mention that, as the motion compensation relies on an assumed set of possible motion models, mismatches between model and actual target motion likely arise when the integration time increases, resulting in integration losses.

To further increase the integration time of the system, Track-Before-Detect (TBD) schemes can be used. Generally, TBD processors are fed with a number of unthresholded data streams and operate energy integrations over admissible target trajectories, after which target tracks giving rise to sufficiently high merit functions are declared [5]-[7]; however, these methods require to discretize the target state space, leading to high computation and memory resource requirements [8]. A different type of TBD scheme considers a pre-processing stage to sensibly reduce the data in input to the TBD processor [9]-[11]. In particular, in [11] Grossi *et al*. proposed an efficient scheme where the TDB processor operates directly on input plot lists avoiding the discretization of the target state space. The two-stage architecture that they proposed consists in a Detector&Plot Extractor (DPE) followed by a TBD processor based on efficient dynamic programming algorithms for the formation of prospective tracks.

In this work, the two-stage architecture in [11] has been specialized for its application in the GNSS-based passive radar system for maritime surveillance. Particularly, the DPE stage consists in the long time MTI technique operating with a properly lowered threshold. The subsequent TBD stage exploits the kinematic parameters evaluated at a number of previous steps, i.e., bistatic range r, Doppler frequency f and Doppler frequency rate $\dot{f}$, to form candidate tracks, whose confirmation is subject to a second thresholding.

The method has been applied against experimental datasets of several minutes exploiting signals transmitted by Galileo satellites and ships of opportunity undergoing different motion

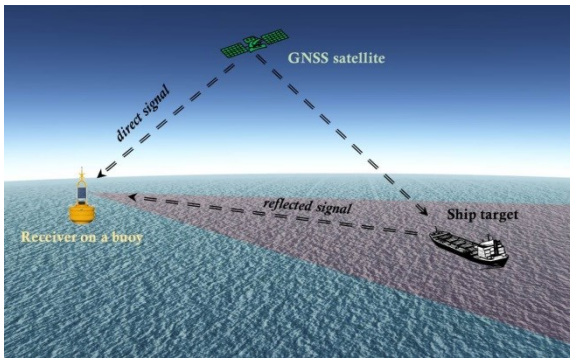

Fig. 1. System concept.

conditions. The provided analysis shows the usefulness of the considered approach in the GNSS-based passive radar to handle long streams of data enhancing the detection capability of the system.

The remainder of this paper is organized as follows. An overview of the system is presented in Section II, while the adopted detection scheme is described in Section III; experimental results are provided in Section IV and conclusions are drawn in Section V.

II. System Overview

Fig. 1 shows a sketch of the considered system. It comprises a GNSS satellite as transmitting source and a receiving-only device (mounted, for example, on the coast or on a moored buoy) equipped with two RF channels: the reference channel, recording the direct satellite signal, and the surveillance channel, collecting the signal reflections from the surveyed area. To enable the detection of the ships navigating in the field of view of the surveillance antenna, an operating scheme as the one reported in Fig. 2 can be adopted. As GNSS signals are CW, a radar data formatting according to an equivalent Pulse Repetition Interval (PRI) – typically selected as the length of the PRN code – has to be preliminary performed.

The considered system falls into the category of bistatic radar and therefore synchronization is required for the subsequent signal processing. In this regard, it should be noted that for the case of GNSS emitters this step can benefit of a full knowledge of the transmitted code, but on the other hand the low SNR in input to the reference channel (that can be as low as –30 dB) makes necessary to resort to ad-hoc signal synchronization algorithms. An overview of one such algorithm is detailed in [1]: the direct signal parameters (delay, Doppler frequency, phase and, if one exists, navigation message) are tracked and exploited to build a noise-free replica of the transmitted signal. This enables the range-compression of the surveillance channel data.

After the range-compression, the sequence of slow-time pulses has to be properly integrated to achieve SNR levels suitable for the detection of the targets. In [1], a basic approach has been considered, by coherently integrating (through slow-time FFT) the pulses inside a time interval short enough to assure constant target reflectivity (typically 2-3 s). This has been shown sufficing for the detection of large targets at relatively short receiver standoffs, but it falls in detecting ships at longer ranges or/and with smaller size.

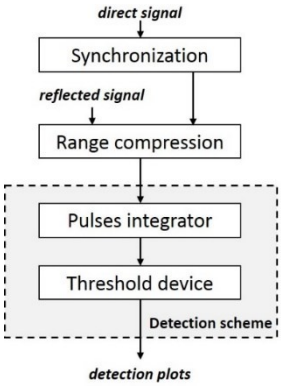

Fig. 2. Operating scheme.

To increase the system performance, in [1] and [2] hybrid coherent/non-coherent integration procedures have been considered. These consist of coherent integrations over consecutive short time frames followed by a quadratic integration. The approaches rely on proper Target Motion Compensation (TMC) procedures to handle the target migration inside the individual frames and among the different frames.

The TMC can take place in the Cartesian plane XY, representing the section of the marine area covered by the radar antenna (local plane-based technique), or in the RD plane (basic plane-based technique). The former can potentially achieve the highest integration gain, but at the cost of a computationally demanding procedure. The basic plane-based technique can implement a more efficient TMC procedure by assuming a linear approximation of the target Doppler history. The performance analysis provided in [2] showed that in many practical applications the local plane-based and the basic plane-based techniques are equivalent, thus being the latter preferable for its lower computational load. In the remainder of the work, we will implicitly refer to the basic plane-based technique as the long-time MTI technique.

In principle, higher detection performance may be obtained with the long-time MTI technique by increasing the number of frames. However, this trivial solution is hampered by a number of reasons. First, it should be pointed out that even though the basic plane-based technique efficiently handles the target migration compensation via a FFT-based procedure, the compensation needs to be executed for a number of motion conditions related to a set of possible target Doppler rates, whose cardinality increases with the number of integrated frames [2]. Moreover, as the motion compensation relies on an assumed set of possible motion models, mismatches between model and actual target motion likely arise when the integration time increases, resulting in integration losses.

An alternative detection scheme based on the TBD paradigm is described in the following section. This is able to achieve longer integration times than the basic plane-based long time MTI technique, at the cost of a negligible increase of the computational complexity.

III. Adopted Detection Scheme

The considered detection scheme, whose block diagram is shown in Fig. 3, consists of a DPE stage followed by a TBD processor [11]. A set of candidate plots is obtained after the integration of the multiple frames addressed during the DPE

stage, which are declared after the subsequent TBD processing over multiple scans.

A. Detection and Plot Extractor

The DPE shall consist of the basic plane-based technique [2], providing for each scan a set of multi-frame RD maps according to a specific set of target Doppler rates, followed by a thresholding stage.

Let us consider a data stream pertaining a scan of duration T_{scan}, which is segmented in N_f consecutive frames of short duration T_f. This imposes a grid of admissible Doppler rates having spacing equal to $1/(N_f \cdot T_f^2)$ and bounds according to the maximum assumed velocity [2]. Let $\dot{f}^*$ be an admissible value of the target Doppler rate, the N_f frames feed the following steps:

Doppler migration compensation – Doppler migration inside each frame and frame to frame are both related to $\dot{f}^*$; they can be compensated by multiplying the data in the range and slow-time domain for a phase ramp comprising both sources of migration.

Range migration compensation – range migration inside each frame can be neglected due to the coarse range resolution. According to the assumed motion model, the range migration experienced over the different frames is composed by a linear term (related to the target Doppler frequency) and by a quadratic term (related to the target Doppler rate). These can be compensated by multiplying each Doppler bin of the data in the fast-frequency and Doppler domain for a phase term comprising both the orders of migration.

Multi-frame integration – the RD maps pertaining the different processed frames and the same Doppler rate are integrated in the intensity domain. A stack of integrated maps $RD(r, f, \dot{f})$ is therefore obtained. Clearly, the maximum gain is obtained in the map pertaining the Doppler rate closest to the actual value.

Then, a proper decision threshold γ_1 is applied to each integrated map (for example by applying a 2D Cell Average Constant False Alarm Ratio CA-CFAR scheme) set in order to achieve a desired level of probability of false alarm P_{fa_1}. Let D_ℓ be the number of alarms at the ℓth scan in the whole stack of RD maps, the corresponding plot list is given by

$$\boldsymbol{S}_\ell = \{\boldsymbol{s}_{1,\ell}, \dots, \boldsymbol{s}_{D_\ell,\ell}\} \quad (1)$$

where $\boldsymbol{s}_{k,\ell}$ contains the range, Doppler frequency and Doppler frequency rate corresponding the kth detected target as well as its intensity $I_{k,\ell}$, namely

$$\boldsymbol{s}_{k,\ell} = (r_{k,\ell}, f_{k,\ell}, \dot{f}_{k,\ell}, I_{k,\ell}) \quad (2)$$

The above procedure is applied to successive time windows here referred to as successive scans. A shift ΔT is considered between two scans. The obtained output lists feed the TBD processor described below.

B. Track-Before-Detect processor

The goal of the TBD processor is correlating the plots in the current plot-list with those in the past L – 1 plot lists, forming a prospective track that can be confirmed or deleted based on the number of plots in the track itself and its strength. As aforementioned, the adopted scheme is closely based on the dynamic programming algorithms proposed in [11], to which we refer for a more detailed description. The main parameters and steps of the processor are here summarized.

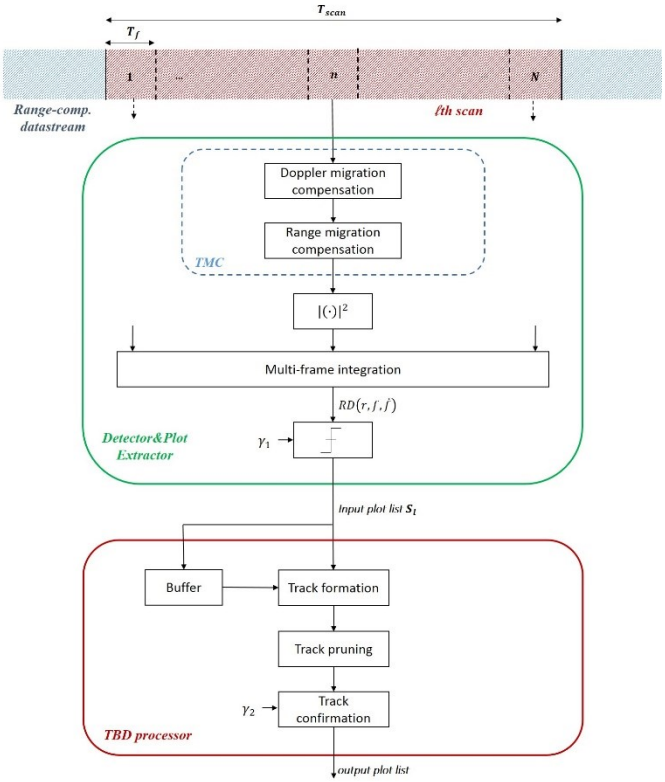

Fig. 3. Adopted detection scheme block diagram.

Track Formation – The plots pertaining the different scans are iteratively associated to form possible trajectories. A trajectory is defined by a vector $\boldsymbol{v} = (v_1, \dots, v_L)$ with $v_\ell \in \{0,1, \dots, D_\ell\}$; $v_\ell = k \neq 0$ means that the alarm $\boldsymbol{s}_{k,\ell}$ belongs to the track $\boldsymbol{v}$, while $v_\ell = 0$ denotes a missing observation. Constraints on the target kinematics rule the formation of a hypothesized $\boldsymbol{v}$, as it will be detailed in the following. Each trajectory is scored by a decision statistic given by the sum of the intensities of the individual plots. The algorithm takes also into account possible missed detections within a track via a parameter P representing the maximum number of consecutive null entries in the vector $\boldsymbol{v}$. In correspondence of a missed detection, an intensity equal to the mean background level (here assumed independent from the frame/scan number) has been here considered.

Track Pruning – After the track formation, some hypothesized tracks may share a common root, i.e., the plot $\boldsymbol{s}_{k,\ell}$ could be associated to different vectors $\boldsymbol{v}$. The track pruning step resolves such ambiguities by assigning the common plots only to the one providing the largest decision statistic. The hypothesized tracks and their decision statistics are correspondingly updated. Subsequently, tracks having a number of non-null entries lower than Q are considered not reliable and therefore deleted.

Track Confirmation – The pruned tracks are finally confirmed or deleted by comparing their decision statistic to a second threshold γ_2 to assure a desired level of false alarm P_{fa_2}.

In order to specialize the algorithms above for the considered scenario, we need to define proper constraints among plots belonging to the different scans for the track formation. Let $\boldsymbol{s}_{h,\ell-p}$ be the last not null entry of an initialized track, where $1 \leq$

$p \leq P+1$. The plot $\boldsymbol{s}_{k,\ell}$ can be linked to $\boldsymbol{s}_{h,\ell-p}$ if it meets requirements on range, Doppler frequency and Doppler frequency rate.

Taking into account the considered target motion model, the expected range position of the plot $\boldsymbol{s}_{h,\ell-p}$ at the ℓth scan time is given by

$$\hat{r}_{h,\ell} = r_{h,\ell-p} - \lambda\, f_{h,\ell-p}\, p\Delta T - \lambda\, \dot{f}_{h,\ell-p}\, \frac{(p\Delta T)^2}{2} \qquad (3)$$

where λ is the wavelength. The expected Doppler position is equal to

$$\hat{f}_{h,\ell} = f_{h,\ell-p} + \dot{f}_{h,\ell-p} p\Delta T \qquad (4)$$

Therefore, the constrains on the range and Doppler position to link plots $\boldsymbol{s}_{k,\ell}$ and $\boldsymbol{s}_{h,\ell-p}$ are given by

$$\begin{cases} {r_{k,\ell}}/{\hat{r}_{h,\ell}} \in [1-m_r;\, 1+m_r] \\ {f_{k,\ell}}/{\hat{f}_{h,\ell}} \in [1-m_d;\, 1+m_d] \end{cases} \qquad (5)$$

where m_r and m_d are proper margins (e.g., a certain number of range and Doppler cells, respectively).

Concerning the Doppler rate, it is assumed that the allowed variation of the Doppler rate measured at the ℓth and at the $(\ell - p)$th scan does not exceed a maximum value set according to the maximum admissible values of the target velocity V_{MAX} and acceleration A_{MAX}, namely

$$\left|\dot{f}_{k,\ell} - \dot{f}_{h,\ell-p}\right| \leq m_{dr} = \frac{3\, V_{MAX}\, A_{MAX}}{\lambda\, r_{h,\ell-p}}\, p\Delta T \qquad (6)$$

It is worth to point out that while m_r and m_d are introduced to handle small deviations between theoretical and actual model of the target kinematics (and possible presence of multiple scattering centers in the case of extended targets), m_{dr} is a large margin needed to overcome the lack of measurements concerning the Doppler rate variation. In this regard, it should be observed that the estimation of the Doppler rate of an alarm is enabled by the long integration time technique adopted at the DPE stage. If the DPE would use a basic short time MTI algorithm as in [1] achieving detection plots over single frame $RD(r,f)$ maps, the constraint over the Doppler history pertaining a prospective track would be weaker. Indeed, it could rely only on physical constraints related to the maximum admissible target speed. In contrast, the exploitation of the multi-frame integration technique results in more reliable tracks in input to the track confirmation stage. This allows to set a lower threshold γ_2 to meet a desired P_{fa_2} than the case in which a short time MTI is employed, so that a higher output probability of detection can be obtained.

It is worth to notice that inserting proper margins in the formation of the prospective tracks allows a higher degree of freedom in the accomplishment of the target energy integration than that allowed by the multi-frame integration, which is based on a precise model of the target motion. Particularly, at the TBD processor stage, the integration path can follow different branches of the Doppler rate bank, not allowed at the DPE stage. Therefore, the adopted scheme is expected to effectively strengthen the target energy even in presence of target motion deviating from the assumed model, for example due to possible maneuvers.

IV. Experimental results

The previously described detection scheme is here validated against experimental data gathered during the measurements campaigns conducted during the H2020 SpyGLASS project [12]. The experimental hardware was placed on a van, which was also equipped with an Automatic Identification System (AIS) receiver to record in real time the actual trajectory of opportunistic targets. The reference channel used a low-gain antenna pointed toward the sky to collect the direct signals of available navigation satellites, while the surveillance channel exploited a high-gain antenna having a beamwidth of about 40°. Particularly, the focus has been on Galileo satellites exploiting the signals transmitted in the E5a band, having a chip-rate (i.e., signal bandwidth) equal to 10.23 MHz.

An acquisition campaign took place in the premises of the Marghera Port (Italy). The receiver acquired the signals scattered by commercial ships leaving or entering in the port terminal. Particularly, the oil tanker Mehmet (130.86m × 17.7m) was in the field of view of the surveillance antenna while it was entering in the port during an acquisition of about 6 minutes. The signal transmitted by the satellite GSAT0214 was tracked during the acquisition. A top view of the acquisition scenario along with the target route provided by the AIS is shown in Fig. 4 (a), while Fig. 4 (b) shows an optical photograph of the target.

After synchronization and range compression, the detection scheme detailed in section III was applied to the whole stream of radar data (350 s). The frame duration is set equal to 3 s, and the DPE operates multi-frame integrations over 10 frames, therefore the scan length is 30 s. An interval equal to 10 s has been considered between consecutive scans, so that 36 input detection lists are available for the TBD processor. From Fig 4 (a) it can be observed that the surveillance antenna Line-of-Sight was roughly superimposed at the naval corridor followed by the vessels, so that a dominant radial motion can be expected; that is to say that the expected target Doppler rate is negligible.

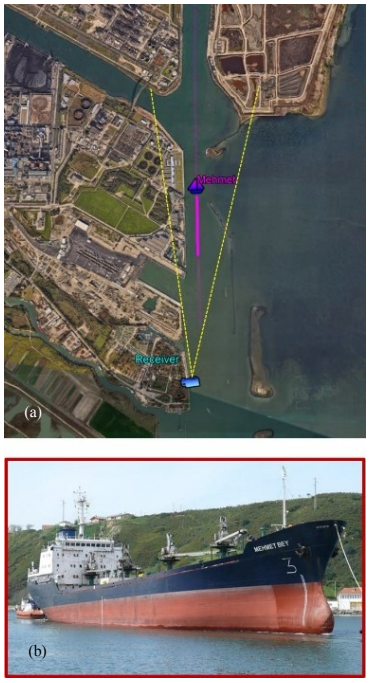

Fig. 4. Marghera port acquisition campaign. (a) Acquisition geometry. (b) Mehmet photograph (from www.marinetraffic.com).

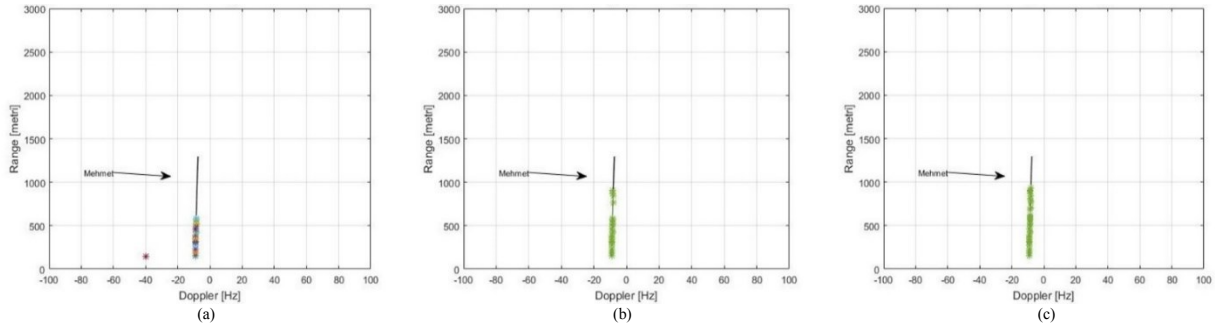

Fig. 5. Mehmet detection results. (a) $P_{fa_1} = 10^{-6}$, TBD not applied. (b) $P_{fa_1} = 10^{-3}$, $P_{fa_2} = 10^{-6}$. (c) $P_{fa_1} = 10^{-2}$, $P_{fa_2} = 10^{-6}$.

Therefore, an *a priori* information concerning the target motion can be exploited to perform the multi-frame integration. Particularly, the TMC implemented at the DPE stage can focus on a single branch of the Doppler frequency rate bank and therefore after the multi-frame integration a unique long-time $RD(r, f, 0)$ map for each scan is obtained.

Fig. 5 shows the obtained detection results. Fig. 5 (a) shows the superimposition of the alarms obtained over successive scans by considering a conventional approach not using the TBD processor. The threshold γ_1 has been set according to $P_{fa_1} = 10^{-6}$. In the initial part of the acquisition, the detected plots follow the target route. Particularly, the target has been detected in the first 20 scans, corresponding to a maximum distance of 600 m. Fig. 5 (b) and (c) concern the case in which the TBD processor has been also considered to increase the detection performance leaving the final false alarm rate equal to 10^{-6}. In Fig. 5 (b), $P_{fa_1} = 10^{-3}$. With respect to the results in Fig. 5 (a), the reduction of the threshold γ_1 provided a larger number of detections after the multi-frame integration, and after the TBD processing (with proper settings of P and Q to assure $P_{fa_2} = 10^{-6}$) the detection rate increased, as it can be observed looking at the alarms in the figure composing the final target track. Fig. 5 (c) shows the obtained track when the DPE false alarm level has been furtherly increased ($P_{fa_1} = 10^{-2}$, whereas P_{fa_2} has been set again equal to 10^{-6}). In this case the target has been detected till its maximum distance from the receiver, equal to 930 m.

As aforementioned, the signal integration carried out by the TBD processor may be effective even in presence of deviation of the target from the assumed trajectory. As a proof of concept experiment, we evaluated the SNR resulting from the integration over an interval equal to 108 s. In a first case, the integration has been completely performed by the DPE considering a set of N_f = 36 frames (T_f = 3 s). In a second case, DPE performs integration over consecutive (non-overlapped) scans of length 12 s, each one segmented in N_f = 4 frames; then, the TBD performs an integration over L = 9 scan. In the former case, the integrated SNR is about 18.5 dB, whereas in the latter it reaches 21 dB. Therefore, an improvement of around 2.5 dB has been obtained thanks to the exploitation of the track formation logic which associates detected plots within a region larger than the resolution cell.

In a second acquisition campaign the receiver was located on the West side of the Venice Lido island (Italy), collecting the signals reflected from waterbuses and passenger ferries sailing in the Venice lagoon. During an about 6 mins long acquisition, the passenger ferry Metamauco (57.85m × 13.1m) was in the field of view of the surveillance antenna, while the signal of the satellite GSAT0212 was correctly tracked. Fig. 6 shows the geometry of the acquisition (comprising the target AIS ground truth) and the target photograph.

Unlike the previous case study, in this scenario not any particular route can been assumed, so that the ship motion can result in any Doppler rate compliant with the maximum target velocity. Therefore, in this case the multi-frame integration has to be accomplished according to a set of possible Doppler rates, resulting for each scan in a set of long-time RD maps. Also in this case, the frame duration has been set equal to 3 s, N_f = 10 and ΔT = 10 s; the target was in the field of view of the radar antenna over 38 successive scans.

Fig. 7 shows the obtained detection results under different processing conditions compared with the AIS ground truth (full line in the figures). In particular, Fig. 7(a) and (b) show the superimpositions of the detection plots obtained over the different scans at the output of the DPE when $P_{fa_1} = 10^{-4}$. The former shows the alarms observed in the RD map corresponding to $\dot{f} = 0$. It can be observed that in this case the plots follow very roughly the target track. The non-negligible variation of the target Doppler results in considerable integration losses when

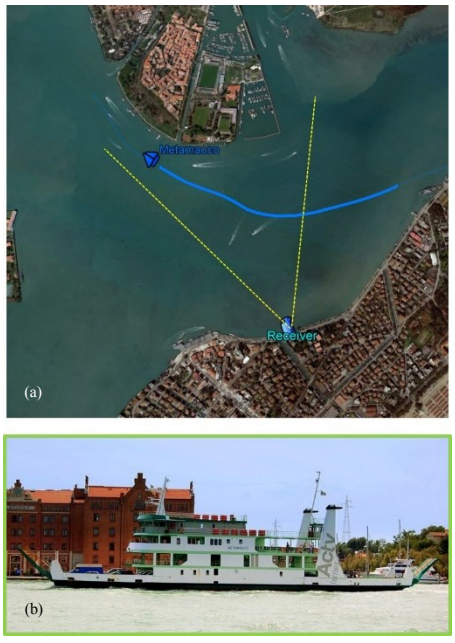

Fig. 6. Venice lagoon acquisition campaign. (a) Acquisition geometry. (b) Metamauco photograph (from www.marinetraffic.com).

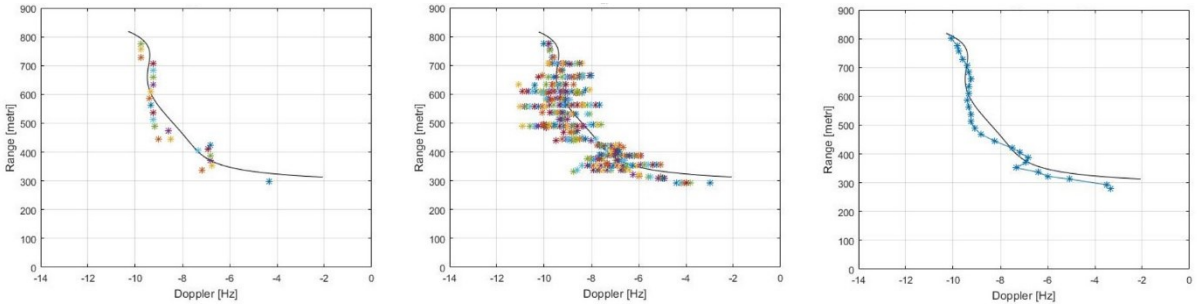

(a) (b) (c)

Fig. 5. Metamauco detection results. (a) Input plot list pertaining RD$(r, f, \dot{f} = 0)$ for $P_{fa_1} = 10^{-4}$. (b) Input plot list pertaining the whole stack of RD$(r, f, \dot{f})$ maps for $P_{fa_1} = 10^{-4}$. (c) Output plot list for $P_{fa_1} = 10^{-2}$ and $P_{fa_2} = 10^{-6}$.

the TMC is performed neglecting the Doppler rate, preventing its detection. In this regard, it can be also noticed that most of target detections occur in the fragment of the track around –9 Hz, where a dominant radial motion has been experienced. Considering all the multi-frame RD maps pertaining the different values of the Doppler rate [Fig. 7 (b)], a richer set of target detections is obtained and it can be observed that alarms occur even in the part of the track in the interval [-3 Hz,-9 Hz], where the target undergoes a dominant tangential motion. Nevertheless, it is worth to point out that in several scans the target gave rise to detections in multiple RD maps (i.e., for different Doppler rates). This can be observed looking at the cluster of plots around the same range positions (e.g., the long clusters around 500 m, 550 m and 600 m). As analyzed in [2], even though the TMC provides the highest integration gain for the Doppler rate closest to the actual target motion, depending on the specific input SNR more maps could result in undesired (ambiguous) detections. A possible solution could be applying proper post detection logic for ambiguity removal; nevertheless, this could entail losses of weaker targets falling in the ambiguity region. Exploiting the TBD processor is an alternative solution, where proper settings of the track formation procedure can result in the formation of an individual track for each target, allowing to follow a trajectory over different branches of the Doppler rate filter. Fig. 7 (c) shows the output plot list after the TBD when $P_{fa_1} = 10^{-2}$ and $P_{fa_2} = 10^{-4}$. It can be observed as a unique and continuous track has been obtained: the lower threshold at the DPE stage allowed for more detections in input at the TBD processor, which inherently operated a rejection of the ambiguities resulting from the multi-frame integration.

V. Conclusions

The GNSS-based passive radar can represent a cost-effective solution for maritime monitoring in both coastal and open sea areas. Nevertheless, the potentialities of the system have to be balanced with a very unfavorable power budget, which requires efforts to improve the detection performance of this technology. In this paper, we considered a combination of long-integration time MTI technique and dynamic programming TBD algorithms to improve the ship targets detectability of the system. The preliminary experimental results here provided clearly show as this approach is effective in the achievement of detection of ship targets of interest under different motion conditions, even comprising target maneuvers, exploiting dwells in the orders of minutes with computation complexity affordable by practical systems.

Acknowledgment

The experimental datasets processed in this work were acquired during the campaigns carried out in the frame of the European Union's Horizon 2020 project "GALILEO-BASED PASSIVE RADAR SYSTEM FOR MARITIME SURVEILLANCE — SpyGLASS", with project consortium composed by Aster S.p.A. (Italy, coordinator), Sapienza University of Rome (Italy), University of Birmingham (UK) and Elettronica GmbH (Germany).

The authors would like to thank Aster S.p.A. for providing the synchronization output. A special thank you to Mr. Renato Merko (Sapienza University of Rome) for the valuable cooperation.

References

[1] H. Ma, M. Antoniou, D. Pastina, *et al*., "Maritime moving target indication using passive GNSS-based bistatic radar," *IEEE Trans. Aerosp. Elec. Syst.*, vol. 54, no. 1, pp-115-130, Feb. 2018.

[2] D. Pastina, F. Santi, F. Pieralice, *et al*., "Maritime moving target long time integration for GNSS-based passive bistatic radar," *IEEE Trans. Aerosp. Elec. Syst.*, vol 54, no. 6, pp. 3060-3083, Dec. 2018.

[3] H. Ma, M. Antoniou, A. G. Stove, J. Winkel, and M. Cherniakov, "Maritime moving target localization using passive GNSS-based multistatic radar," *IEEE Trans. Geosci. Remote Sens*., vol. 56, no. 8, pp. 4808-4819, Aug. 2018.

[4] F. Santi, F. Pieralice, D. Pastina, "Joint detection and localization of vessels at sea with a GNSS-based multistatic radar," *IEEE Trans. Geosci. Remote Sens.*, in press.

[5] Y. Barniv, "Dynamic programming solution for detecting dim moving targets," *IEEE Trans. Aerosp. Elec. Syst*., vol. 21, no. 1 pp. 144-156, Jan. 1985.

[6] S. M. Tonissen, and Y. Bar-Shalom, "Maximum likelihood track-before-detect with fluctuating target amplitude," *IEEE Trans. Aerosp. Elec. Syst.*, vol. 34, no. 3 pp. 796-809, Jul. 1998.

[7] M. G. S. Bruno, and J. M. F. Moura, "Multiframe Detector/Tracker: Optimal Performance," *IEEE Trans. Aerosp. Elec. Syst.*, vol. 37, no. 3 pp. 925-945, Jul. 2001.

[8] S. J. Davey, M. G. Rutten, and B. Cheung, "A comparison of detection performance for several track-before-detect algorithms," *2008 11th Int. Conf. Information Fusion*, Cologne, 2008, pp. 1-8.

[9] B. D. Carlson, E. D. Evans, and S. L. Wilson, "Search radar detection and track with the Hough trasnform. Part I: system concept," *IEEE Trans. Aerosp. Elec. Syst.*, vol. 30, no. 1 pp. 102-108, Jan. 1994.

[10] S. Buzzi, M. Lops, and L. Venturino, "Track-before-detect procedures for early detection of moving target from airborne radars," *IEEE Trans. Aerosp. Elec. Syst.*, vol. 41, no. 3 pp. 937-954, Jul. 2005.

[11] E. Grossi, M. Lops, and L. Venturino, "A novel dynamic programming algorithm for track-before-detect in radar systems," *IEEE Trans. Signal Process*., vol. 61, no. 10, pp. 2608-2619, May 2013.

[12] spyGLASS – GALILEO-BASED PASSIVE RADAR SYSTEM FOR MARITIME SURVEILLANCE, 2015. [Online]. Available: www.spyglassproject.eu.